Biogeosciences Discuss., 12, 9905–9934, 2015
www.biogeosciences-discuss.net/12/9905/2015/
doi:10.5194/bgd-12-9905-2015

Biogeosciences Discussions
Open Access

Thermocline mixing and vertical oxygen fluxes in the stratified central North Sea

L. Rovelli[1,a], **M. Dengler**[1], **M. Schmidt**[1], **S. Sommer**[1], **P. Linke**[1], and **D. F. McGinnis**[1,2]

[1]GEOMAR Helmholtz Centre for Ocean Research Kiel, Kiel, Germany
[2]Institute F.-A. Forel, Faculty of Science, University of Geneva, Carouge, Switzerland
[a]now at: Scottish Association for Marine Sciences (SAMS), Oban, UK

Received: 24 April 2015 – Accepted: 15 June 2015 – Published: 03 July 2015

Correspondence to: L. Rovelli (lorenzo.rovelli@sams.ac.uk)

Published by Copernicus Publications on behalf of the European Geosciences Union.

Abstract

In recent decades, the central North Sea has been experiencing a general trend of decreasing dissolved oxygen (O_2) levels during summer. To understand the potential causes driving lower O_2, we investigated summertime turbulence and O_2 dynamics in the thermocline and bottom boundary layer (BBL). The study focuses on coupling biogeochemical processes with physical transport processes to identify key drivers of the O_2 and organic carbon turnover within the BBL. Combining our flux observations with an analytical process-oriented approach, we resolve the key drivers that ultimately determine the BBL O_2 levels. We report substantial tidally-driven turbulent O_2 fluxes from the thermocline into the otherwise isolated bottom water. This contribution to the local bottom water O_2 and carbon budgets has been largely overlooked and might be a central factor maintaining relatively high O_2 levels in the bottom water throughout the stratification period. With the current climate warming projections, we propose that higher water temperature and reduced turbulence could favour migrating algal species that could out-compete other species for light and nutrients, and shift the oxygen production zone higher up within the thermocline while maintaining similar organic carbon export to the bottom water. Due to the substantially lower turbulence levels in the central region of the thermocline as compared to the higher turbulence observed at the thermocline-BBL interface, such a shift in the production layer could lead to further isolation of the bottom water and promote the seasonal occurrence of lower O_2 concentrations.

1 Introduction

1.1 Oxygen dynamics in marine systems

The distribution of dissolved oxygen (O_2) in marine systems results from the complex interaction between biological processes (photosynthesis and respiration) and physical

BGD
12, 9905–9934, 2015

processes (O_2 flux pathways) occurring within the water column and at the seafloor. O_2 is therefore regarded as an important indicator of ecosystem functioning for aquatic organisms (Best et al., 2007) as well as for benthic activity (e.g., Glud, 2008). Changes in the O_2 distribution and supply to the deeper waters are tightly linked to ocean warming and eutrophication, highlighting the need to understand the physics driving the O_2 fluxes (Joos et al., 2003).

O_2 concentrations below 62.5 µmol L^{-1} (i.e., hypoxic regime) (Vaquer-Sunyer and Duarte, 2008) can produce significant stress on aquatic communities leading to increased mortality among fish communities (Diaz, 2001), thus highlighting the ecological and economical impacts of O_2 depletion. As reviewed by Diaz and Rosenberg (2008), hypoxia in coastal environments is spreading and so are the reports of unprecedented occurrence of hypoxia in several shelf seas and coastal regions (Grantham et al., 2004; Chan et al., 2008; Crawford and Pena, 2013).

1.2 Oxygen distribution in the North Sea

Eutrophication and climate change effects on the North Sea are a major concern. Since 1984, surface water temperatures in the North Sea have increased by 1–2 °C, greater than the global mean (OSPAR, 2009, 2010; Meyer et al., 2011). On seasonal time scales, climate projections indicate an earlier start of stratification, longer duration, and stronger thermocline stability (Lowe et al., 2009). Due to the semi-enclosed nature of the North Sea, earlier onset and longer stratification increases the length of time that the deep water is isolated, allowing lower O_2 concentrations to develop (Greenwood et al., 2010). Indeed, the occurrence of potential ecosystem-threatening low O_2 levels has already been reported in the past (e.g., North Sea Task Force, 1993; Greenwood et al., 2010). While the reported O_2 levels were still above the hypoxic threshold, growing concerns of hypoxia developing in the North Sea have highlighted the need for more detailed studies on the O_2 dynamics and driving forces (Kemp et al., 2009).

BGD
12, 9905–9934, 2015

1.3 Controls on oxygen dynamics

The distribution of O_2 and the other dissolved constituents within aquatic systems are largely dictated by physical transport processes, with turbulent transport significantly contributing to constituent balances (see Rippeth, 2005; Fischer et al., 2013; Kreling et al., 2014). In shelf seas such as the North Sea, the seasonal occurrence of steep thermoclines acts as an important physical barrier separating the surface layer from nutrient-rich deeper waters (Sharples et al., 2001). As measurements of shear and stratification have shown that the central North Sea thermocline is in a state of marginal stability (van Haren et al., 1999), additional sources of shear could trigger shear instability leading to local production of turbulence within the thermocline. This enhanced local turbulence would subsequently enhance the vertical exchange of constituents such as O_2, organic carbon and nutrients. Therefore, resolving the processes that drive diapycnal (i.e., vertical) fluxes across the thermocline throughout the stratification period is key to understanding the biogeochemical functioning of shelf seas (e.g., Sharples et al., 2001).

1.4 Present study

The goal of this study is therefore to quantify key turbulent processes driving the O_2 fluxes across the thermocline, with the emphasis on the bottom water O_2 balance. We investigate and describe key processes driving the O_2 flux to the bottom waters, and how this will influence the seasonal O_2 balance. Using the resolved O_2 flux, we perform a simple 1-D mass balance model to quantify the O_2 sources and sinks, and loss in the water column. Finally, we propose processes that could promote hypoxia development in the central North Sea in a warming climate.

BGD
12, 9905–9934, 2015

2 Methods

2.1 Study site

We performed our O_2 and turbulence measurements campaign in the Norwegian sector of the central North Sea, N. 1/9, at the Tommeliten site (56°29′30″ N, 2°59′00″ E; Fig. 1) over a time period of three days during the stratification period (8–11 August 2009) aboard the R/V *Celtic Explorer* (cruise CE0913). The site, located ∼ 50 km northeast from the northern Dogger Bank, and its surroundings are characterized by shallow waters (∼ 70 m) at a relatively long distance from coastal areas (on average ∼ 300 km). The site is known for the presence of buried salt diapirs, methane (CH_4) seeps and bacterial mats (Hovland and Judd, 1988). Bathymetric surveys from Schneider von Deimling et al. (2010) revealed a rather flat sandy seabed with almost no features, with the exception of cm-sized ripples (McGinnis et al., 2014).

The currents of the central North Sea are predominantly driven by the semi-diurnal lunar tide (M_2; Otto et al., 1990). Seasonal stratification starts in April around Julian day 100 (e.g., Meyer et al., 2011). The thermocline has been identified as an important zone for the establishment of primary production and the O_2 maximum layer (see Pingree et al., 1978). In fact, the North Sea deep chlorophyll maximum (DCM) is estimated to account for 58 % of the water column primary production and 37 % of the annual new production for the summer stratified North Sea (Weston et al., 2005). The development of the associated O_2 maximum due to this production is thus important and so far not considered in the overall O_2 balance of the central North Sea.

2.2 Instrumental setup

High resolution (mm scale) turbulent shear and temperature profiles were obtained with a MSS90-L (Sea and Sun Technology, Trappenkamp, Germany) microstructure turbulence profiler. The MSS90-L is a free-falling, loosely-tethered profiler which samples at 1024 Hz with 16 channels and is designed for an optimal sink rate of 0.5–0.6 m s^{-1}.

BGD
12, 9905–9934, 2015

The probe was equipped with two air-foil shear probes, an accelerometer (to correct for probe pitch, roll, and vibration), a fast temperature sensor (FP07, 7–12 ms response time), standard CTD sensors (temperature, pressure, conductivity), and a fast (0.2 s response time) galvanic O_2 sensor (AMT, Analysenmesstechnik GmbH, Rostock, Germany). The absolute O_2 concentrations were calibrated against shipboard CTD O_2 profiles and Winkler titrations on discrete water samples (see below).

Water column hydrodynamics were characterized with the compact benthic Paleoceanography (POZ) lander, which was deployed using a video guided launcher (Pfannkuche and Linke, 2003). The POZ lander recorded 3-dimensional current velocity profiles and acoustic backscatter information throughout the water column using a 300 kHz acoustic Doppler current profiler (ADCP; Workhorse Sentinel, Teledyne RD Instruments, Poway, United States), which sampled every 15 s with a bin size of 0.5 m starting from 2.75 m from the bottom. A conductivity-temperature-depth (CTD) logger (XR-420 CT logger, RBR, Kanata, Canada) recorded temperature, conductivity and pressure (Digiquarz, Paroscientific, Redmond, USA) every 2 s near the seafloor (~ 0.3 m distance).

Water column profiles were obtained using a SBE9plus CTD-rosette system (Seabird, Washington, USA). The CTD sampled at 24 Hz and was equipped with standard temperature, conductivity, pressure, O_2 and light transmission sensors. The rosette system mounted 12 10 L-Niskin-bottles for discrete water sampling.

2.3 Hydrodynamic data evaluation

The main tidal directions, the major and minor axis of the tidal ellipsoid, were determined by performing a variance analysis on the ADCP velocity time series. The u and v velocities were rotated over a stepwise increasing rotation angle (r) as $u_{\mathrm{rot}} = u \cdot \cos(-r) - v \cdot \sin(-r)$ respectively $v_{\mathrm{rot}} = u \cdot \sin(-r) - v \cdot \cos(-r)$, and the variance computed at each step. The angle at the largest variance represented the main tidal direction. Barotropic and baroclinic flow contributions of tides were separated by least-square fitting the detrended velocity time series to harmonics $u = A \cdot \cos(\omega \cdot t + \varphi)$ with

BGD
12, 9905–9934, 2015

A, ω, ϕ being the amplitude, frequency, and the phase lag, respectively. In the analysis below, the barotropic semi-diurnal principle lunar tide (M_2) and diurnal declination tide (K_1) contributions had frequencies of 1.93227 and 1.00274 cpd (cycles per day), respectively, and were subtracted from the time series to analyze residual flow. For barotropic contributions, the fit was applied to the depth average of the time series, while baroclinic contributions were obtained by fitting the harmonics to the velocity time series from each 0.5 m ADCP bin. The occurrence of enhanced shear in the stratified water column was investigated by calculating the vertical shear of horizontal velocity, S, from the vertical gradients between adjacent bins of east and north velocity (0.5 m resolution) as $S = \sqrt{(\mathrm{d}u/\mathrm{d}z)^2 + (\mathrm{d}v/\mathrm{d}z)^2}$. Frequency spectra of the time series of horizontal velocity and vertical shear of horizontal velocity were used to identify the tidal and non-tidal flow components. The spectra were calculated using fast-Fourier transforms combined with a 1/2-cosine tapper (Hanning window) that was applied to the first and last 10 % of the time series data.

Turbulent kinetic energy dissipation rate (ε) was quantified from the airfoil shear readings by integrating shear wavenumber spectra assuming isotropic turbulence (Batchelor, 1953):

$$\varepsilon = 7.5\mu \int_{k_{\min}}^{k_{\max}} E_{\mathrm{d}u'/\mathrm{d}z}(k)\mathrm{d}k \quad (1)$$

where μ is the dynamic viscosity of seawater. Shear spectra $E_{\mathrm{d}u'/\mathrm{d}z}(k)$ were calculated from one-second ensembles (1024 values) and integrated between a lower $k_{\min}$ = 3 cpm (cycles per minute) and an upper wavenumber $k_{\min}$ that varied between 14 and 30 cpm depending on the Kolmogorov wavenumber. Here, a Bartlett window was applied to the whole ensemble prior to spectral decomposition. Loss of variance due to the limited wavenumber band was taken into account by fitting the observed shear spectra to the universal Nasmyth spectrum. Similarly, corrections for the loss of variance due to finite sensor tip of the airfoil probes were applied (see Schafstall et al.,

BGD
12, 9905–9934, 2015

2010). The detection limit, or noise level, of the used profiler for ε was inferred to be $1 \times 10^{-9}\,\mathrm{W\,kg^{-1}}$ (Schafstall et al., 2010); the upper detection limit is a function of the shear sensor geometry (up to $10^{-4}\,\mathrm{W\,kg^{-1}}$; Prandke and Stips, 1998).

Estimates of the turbulent eddy diffusivities of mass (K_ρ) were obtained from measurements of ε as

$$K_\rho = \frac{\gamma \varepsilon}{N^2} \tag{2}$$

where γ is the mixing efficiency and N^2 the water column stability. This method, proposed by Osborn (1980), approximates K_ρ under the assumption of a local equilibrium of production and dissipation of turbulent kinetic energy. Values for N^2 were calculated from temperature, salinity and pressure data using the adiabatic method (Fofonoff, 1985) as $N^2 = -g(\rho^{-1}\partial\rho/\partial z - g/c^2)$, where ρ, g, and c are the density, the earth's gravitational acceleration and speed of sound, respectively. Mixing efficiency values in stratified waters range from 0.1 to 0.2 (Ivey and Imberger, 1991) and decreases in weakly stratified waters such as within the BBL (Lorke et al., 2008). To account for this decrease, we used the γ and K_ρ parameterization of Shih et al. (2005). Based on the turbulence activity parameter $\varepsilon/\upsilon N^2$, with the kinematic viscosity, υ, the authors found that in energetic regimes, i.e., $\varepsilon/\upsilon N^2 > 100$, the eddy diffusivities are better estimated as $K_\rho = 2\upsilon(\varepsilon/\upsilon N^2)^{1/2}$. As horizontal density gradients at the study site were small compared to vertical gradients, we equated diapycnal eddy diffusivities with vertical diffusivities (i.e., $K_\rho = K_z$).

To obtain representative mean turbulent eddy diffusivities, the data were evaluated in ensembles of three to four consecutive profiles and averaged in depth and time to reduce uncertainties due to the patchiness of turbulence, temporal fluctuation of N^2, as well as temporal γ variations (see Smyth et al., 2001). As proposed by Ferrari and

BGD
12, 9905–9934, 2015

Polzin (2005), the level of uncertainty of the averaged K_z can be quantified as:

$$\Delta K_z = K_z \left[\left(\frac{\Delta\gamma}{\gamma} \right)^2 + \left(\frac{\Delta\varepsilon}{\varepsilon} \right)^2 + \left(\frac{\Delta N^2}{N^2} \right)^2 \right]^{1/2} \quad (3)$$

with Δ being the absolute uncertainty of the various average terms. Here, the uncertainties are evaluated in the region of strong vertical O_2 gradients and in 2 m depth bins. The absolute uncertainty $\Delta\gamma$ was assumed to be 0.04 (see St. Laurent and Schmitt, 1999). The absolute uncertainty for N^2 (ΔN^2) was determined by the standard error over the 2 m average, computed as the standard deviation divided by the square root of the number of estimates. Finally, the statistical uncertainty for ε for each bin was calculated using a bootstrap method (10^4 resamples) (Efron, 1979).

The vertical O_2 fluxes F_θ were then obtained from K_z and the O_2 concentration gradients $\partial[O_2]/\partial z$ as

$$F_\theta = K_z \frac{\partial[O_2]}{\partial z} \quad (4)$$

Accordingly, the uncertainty of averaged turbulent O_2 fluxes were given by:

$$\Delta F_\theta = F_\theta \left[\left(\frac{\Delta K_z}{K_z} \right)^2 + \left(\frac{\Delta\partial_z[O_2]}{\partial_z[O_2]} \right)^2 \right]^{1/2} \quad (5)$$

where $\Delta\partial_z[O_2]$ denotes the standard error of mean vertical gradients of O_2 concentrations. It should be noted that the analysis did not include biases or uncertainties due to measurement errors.

3 Results

During the three-day observational period (8–11 August 2009) we collected 39 high-resolution MSS profiles in sets of three to five profiles that were collected consecutively

BGD
12, 9905–9934, 2015

at 5–10 min intervals. Most of the profiles were collected either in the evening (profiles 1–8, 26–28, 36–39) or at night (9–15, 29–35) with the remaining profiles acquired in the morning (6 to 9 a.m.). One shipboard CTD profile was performed prior to the actual MSS profiles to provide oceanographic background information, the water turbidity and O_2 concentrations, as well as discrete water samples for subsequent onboard Winkler titrations. Hydroacoustic water column current measurements were carried out continuously throughout the observational period. The following results are structured to first present a characterization of the site's physical settings and turbulence drivers, followed by the O_2 fluxes and O_2 BBL budget.

3.1 Water column structure

The ~ 70 m deep water column was characterized by a stable, well-defined four-layer temperature structure (Fig. 2a). A well-mixed surface boundary layer (SBL) and bottom boundary layer (BBL), 15 and 30 m thick, respectively, were separated by a weakly-stratified transition layer (15–25 m depth) and a strongly stratified interior layer (25–40 m depth). The stratified interior layer was characterized by two very steep thermoclines situated in the upper (27–30 m depth) and lower (36–39 m depth) region of the layer, with vertical temperature gradients of up to 4 °C m^{-1}. The average salinity was 35.08 with little variation throughout the water column (35.04–35.1). The light transmission profile from the ship CTD ranged from 89 to 96 % (Fig. 2b). The most turbid layer (89 %) was observed at the lower boundary of the interior layer (at 40 m depth) suggesting the presence of the deep chlorophyll maximum, phytoplankton, zooplankton and suspended particles.

The O_2 profiles were generally characterized by near saturation in the SBL and transition layers, and an undersaturated (~ 80 %) BBL (Fig. 2c). The stratified interior was oversaturated by up to 115 %, with a well-established O_2 maximum at ~ 39 m depth with concentrations up to ~ 315 µmol kg^{-1} (Fig. 2d). Below that maximum, at the thermocline-BBL interface, we observed a 2–3 m thick steep oxycline, with an O_2

BGD
12, 9905–9934, 2015

gradient of 34 µmol kg^{-1} m^{-1} with exhibited limited day–night, depth and thickness variability. With this in mind, we wish to resolve the O_2 flux into the BBL associated with the oxycline.

3.2 Hydrodynamics

The POZ lander hydrostatic pressure dataset revealed that the tidal water level ranged from 0.6 to 0.9 m (Fig. 3a). Variance analysis on the ADCP velocity data identified the major and minor axis of the tidal ellipsoid components to occur at 45 and 135° from true north, respectively. Along these axes, the current amplitudes were 0.21 and 0.04 m s^{-1}, indicating a narrow tidal current ellipsoid, as reported by Otto et al. (1990). The site was characterized by a negative tide polarity (anti-cyclonic) for the semi-diurnal tides. A dominance of the barotropic M_2 current amplitude at all depths was also clearly observed in the velocity time series (Fig. 3b and c) and the harmonic analyses. East (zonal) and north (meridional) barotropic M_2-current amplitudes were 0.12 and 0.17 m s^{-1}, respectively, while K_1-current amplitudes were only 0.005 and 0.03 m s^{-1}.

Superimposed on the barotropic currents, we observed the presence of baroclinic velocity contributions (Fig. 3b and c). Although the limited length of the ADCP velocity time series did not allow for full separation of the M_2 and f frequencies, the spectral density functions indicated maximum energy at frequencies of about the semi-diurnal tide. This maximum varied little with depth indicating barotropic M_2 motions. Superimposed on those barotropic currents, we observed the presence of baroclinic velocity contributions (Fig. 3b and c). Additionally, near-inertial motions were also observed.

The occurrence of near-inertial motions was most pronounced in the thermocline (32–39 m; Fig. 3e). Lower but still elevated energy densities at the near-inertial band were also found in the SBL and BBL. Moreover, the near-inertial currents exhibited a distinct 180° phase shift between the SBL and the thermocline as well as between the thermocline and the BBL, suggesting a second vertical mode nature of these fluctuations. Average amplitudes of the near-inertial fluctuations in the thermocline obtained

BGD
12, 9905–9934, 2015

from least-square fitting were 0.11 $m\,s^{-1}$. In the BBL and SBL, average amplitudes were reduced to 0.06 and 0.04 $m\,s^{-1}$, respectively, suggesting that f oscillations might account for enhanced shear in the thermocline.

Enhanced vertical shear of horizontal velocity was found at the interior–transition layer as well as at the interior–BBL interfacial regions (Fig. 3d). As indicated by the spectral density function of the shear time series from the interior interfacial layers (not shown), the shear exhibited near-inertial frequencies (1.6722 cpd), and resulted from the baroclinic near-inertial wave. The high vertical resolution (0.5 m) of our velocity data allowed the resolution of the interfacial shear layers, which were typically 2 to 3 m thick with elevated values of up to 0.05 s^{-1}. Comparisons with CTD data showed that they are collocated with the two enhanced temperature gradients layers in the thermocline (27–30 m and 36–39 m depth; Fig. 2a).

The dissipation rates (ε) of turbulent kinetic energy (TKE) determined from microstructure shear probes were particularly low ($2–5 \times 10^{-9}$ $W\,kg^{-1}$) but above the MSS detection limit in the center of the stratified interior. However, TKE increased to 5×10^{-9} and 2×10^{-8} $W\,kg^{-1}$ at the upper and lower interior layer limits, respectively (Fig. 4a). These coincided with the depth range of the interfacial shear layers (Fig. 3d) at the strong temperature gradients (Fig. 2a) and resulting water column stability maxima ($\sim 1 \times 10^{-3}$ s^{-2}).

Bin-averaged values of K_z varied by a factor of 5, ranging from 6×10^{-7} $m^2\,s^{-1}$ in the central interior to 3×10^{-6} $m^2\,s^{-1}$ in the lower region of the transition layer (Fig. 4b). In the upper interface (thermocline–transition layer), where ε was elevated with respect to the central interior but reduced compared to the lower interfacial layer (Fig. 6), stronger stratification (i.e. larger N^2 values up to 10^{-3} s^{-2}) reduced the eddy diffusivities. At the interior-BBL, higher K_z values ($\sim 2 \times 10^{-5}$ $m^2\,s^{-1}$) resulted from increased turbulence and weaker stratification. This enhanced turbulent transport was located where the vertical O_2 gradient was the strongest (Fig. 2d).

BGD
12, 9905–9934, 2015

3.3 Oxygen fluxes and budget

With the fast responding AMT galvanic O_2 sensor and rapid sampling rate, we were able to resolve the O_2 gradient with a very high precision. Figure 4c shows the 2 m bin average O_2 fluxes for the interior together with the averages from each ensemble. Small O_2 fluxes ($\sim 1\,\mathrm{mmol\,m^{-2}\,d^{-1}}$) were estimated for the center and upper region of the interior; this suggested that relatively little O_2 is transported upward from the O_2 maximum to the rest of the interior. In contrast, a substantial O_2 flux divergence ranging from 9–134 $\mathrm{mmol\,m^{-2}\,d^{-1}}$ (average of 54 $\mathrm{mmol\,m^{-2}\,d^{-1}}$) was identified from the lower thermocline towards the BBL. The confidence interval associated with the uncertainties of the O_2 flux estimates was 18–74 $\mathrm{mmol\,m^{-2}\,d^{-1}}$. Although the O_2 fluxes to the BBL water from the thermocline were variable in magnitude (Fig. 4c), and the measurements limited to the observational period (Fig. 3), their magnitude nevertheless suggests an important, yet overlooked, O_2 pathway.

We performed a simple 1-D BBL mass balance to investigate the relevance to the local O_2 balance. Here, we defined the apparent (measured) O_2 loss rate in the BBL $\partial[O_2]/\partial t$ as the consequence of O_2 replenishment from F_θ and the O_2 utilization via sediment O_2 uptake rate (SUR) and water column organic matter respiration (R) expressed as

$$\frac{\partial[O_2]}{\partial t}\frac{V}{A} = |F_\theta| - |\,\mathrm{SUR}\,| - |R| \quad \{\mathrm{mmol\,m^{-2}\,d^{-1}}\} \tag{6}$$

The mass balance was constrained to the (assumed) well-mixed 35 m deep BBL section of area, $A = 1\,\mathrm{m^2}$ with a volume, $V = 35\,\mathrm{m^3}$. We further assumed negligible horizontal O_2 gradients (as observed from the CTD casts), and thus a net zero horizontal O_2 advective transport.

The average SUR for the same time period and location obtained from parallel eddy correlation measurements, was $\sim -10\,\mathrm{mmol\,m^{-2}\,d^{-1}}$ (McGinnis et al., 2014). Concurrently, the apparent BBL O_2 loss of $-0.42\,\mathrm{\mu mol\,kg^{-1}\,d^{-1}}$ was determined from the POZ O_2 time series. Expressed as a rate with the V/A ratio, the apparent BBL O_2

BGD
12, 9905–9934, 2015

loss was about $-15\,\mathrm{mmol\,m^{-2}\,d^{-1}}$ and thus comparable with the nearby Dogger Bank average presented by Greenwood et al. (2010). Based on Eq. (6) and using the observed BBL O_2 loss rate, F_θ and SUR, the water column respiration, R was calculated to be $\sim -60\,\mathrm{mmol\,m^{-2}\,d^{-1}}$. This implies that without the O_2 replenishment, the apparent BBL O_2 loss would be $\sim -2\,\mathrm{\mu mol\,kg^{-1}\,d^{-1}}$ and thus four times higher than observed. Our results indicated that the total respiration in the bottom water was therefore $\sim -70\,\mathrm{mmol\,m^{-2}\,d^{-1}}$ (SUR + R), with about 14 % of the organic carbon mineralization occurring at the sediment and 86 % in the bottom water column.

4 Discussion

The importance of determining the turbulent processes and accurately resolving the O_2 gradient is immediately apparent for the O_2 interior dynamics and budget within the North Sea. The formation of the O_2 maximum zone due to primary production at the base of the thermocline and the turbulence interactions have significant implications for the O_2 flux to the BBL. This leads to several important insights regarding the local O_2 and carbon budgets within the system. Within this context, we will: (1) discuss the turbulent mechanisms leading to these thermocline O_2 fluxes and those promoting the formation of the O_2 maximum zone in terms of primary productivity, (2) discuss the implication for the local O_2 BBL dynamics and carbon budget, (3) speculate on factors that can ultimately influence O_2 depletion in the North Sea and other seasonally stratified shelf seas.

4.1 Thermocline mixing

The expansive North Sea thermocline ($5 \times 10^5\,\mathrm{km^2}$; Meyer et al., 2011) has been regarded as being in a state of marginal stability, where additional sources of shear could lead to increased thermocline mixing (e.g., van Haren et al., 1999). Itsweire et al. (1989) showed that layers of strong shear are likely to be found where strong stratification oc-

BGD
12, 9905–9934, 2015

curs. In general, away from varying topography, the major sources of shear in the thermocline are considered to be internal tides and near-inertial oscillations (see Rippeth, 2005). Sharples et al. (2007) demonstrated that internal tidally-driven thermocline mixing also enhanced diapycnal nutrient fluxes, the overall productivity in the thermocline, as well as the associated carbon export to the BBL.

The occurrence of near-inertial oscillations in shelf seas during the stratified season has been reported in several studies from the North Sea (van Haren et al., 1999; Knight et al., 2002) as well as in other shelf seas (e.g., Rippeth et al., 2002; McKinnon and Gregg, 2005). During the presence of baroclinic inertial waves in the water column, periods of enhanced shear taking the form of shear spikes occuring approximately every inertial period and in bursts lasting several days have been observed in the western Irish Sea (Rippeth et al., 2009), the Celtic Sea (Palmer et al., 2008) and the northern North Sea (Burchard and Rippeth, 2009). During our observational period, we found that the baroclinic near-inertial wave in the interior was the main contributor to the detected enhanced shear (Fig. 3d) and we proposed it to be the primary source of mixing in an otherwise well-stratified layer.

While we mainly attributed the observed enhanced turbulent mixing to the occurrence of a near-inertial wave, the site's physical setting has further implications for mixing processes in the thermocline. In the Northern Hemisphere, sites with anti-cyclonic tides, such as Tommeliten, are often characterized by an increased vertical extension of the BBL, and higher BBL dissipation rates than comparable cyclonic sites (see Simpson and Tinker, 2009). As a result of this enhanced BBL thickness, we observed sporadically elevated thermocline turbulence resulting from tidal-driven bottom turbulence propagating vertically to the thermocline (data not shown). A study by Burchard and Rippeth (2009) also reported that short lived thermocline shear spikes can arise due to the alignment of the surface wind stress, bulk shear, and bed stress vectors in the presence of baroclinic near-inertial motions and barotropic tidal currents. These mechanisms are stronger with anti-cyclonic tides. While the two-layer mechanism described by these authors would require a more complex structure to be applicable to the Tom-

BGD
12, 9905–9934, 2015

meliten site, all the features required for shear spike generation were present during the observational period.

4.2 BBL O_2 dynamics

Ultimately, observed O_2 depletion in the bottom mixed layer of the North Sea depends on the supply of organic matter, the rate of carbon mineralization, and the flux of O_2 to the bottom water. Our study investigates the significance of the O_2 flux to the BBL, which has been previously overlooked in shelf sea carbon balances. To our knowledge, the only studies focusing on O_2 replenishment in the BBL through the thermocline are limited to freshwater systems (e.g. Bouffard et al., 2013; Kreling et al., 2014). In a large stratified water body such as Lake Erie, O_2 transport from the thermocline to the hypolimnion was found to be substantial, with a magnitude comparable to ∼ 18 % of the hypolimnetic O_2 utilization rate over the whole stratification period (Bouffard et al., 2013). Based on the above, we can argue that the summer O_2 dynamics are more complicated than previously regarded, as the excess of O_2 in the thermocline must also be supported by appropriate nutrient entrainment from the bottom water. The resulting increase in productivity and subsequent export to the bottom water therefore boosts the carbon turnover estimates substantially.

Using a 1 : 1 O_2 utilization–carbon re-mineralization (see Canfield, 1993), Greenwood et al. (2010) inferred the average BBL carbon re-mineralization rate at the nearby North Dogger to be 15 mmol m^{-2} d^{-1}, or 180 mg C m^{-2} d^{-1}. Similar results for a typical NW European shelf sea were obtained via modeling by Sharples (2008), who reported rates ranging from ∼ 35 to ∼ 200 mg m^{-2} d^{-1} for neap and spring tide, respectively. Their study, however, did not include the daily tidal variation, and thus rates could be much higher on shorter timescales.

With the absence of targeted long-term studies focusing on O_2 and carbon dynamics in the thermocline and BBL, we can only speculate on the long-term fate of the BBL O_2 and its replenishment from the thermocline by vertical O_2 fluxes (F_θ). However, it seems possible that the overall net BBL water column O_2 respiration, R, is higher

BGD
12, 9905–9934, 2015

than previously thought, suggesting a much higher carbon turnover than inferred from the apparent O_2 loss rate. Based on Eq. (6), the BBL carbon re-mineralization (and export to the BBL) would be on the order of nearly 850 mg C m^{-2} d^{-1}, almost a factor of 5 higher than reported by Greenwood et al. (2010). However, the same turbulent transport that supports the O_2 export from the DCM to the BBL also supports BBL nutrient import to the DCM (Fig. 5). The higher import of nutrients to the DCM likely promotes additional primary production and a subsequent increase in organic matter (OM) export to the BBL. In such a scenario, the ephemeral O_2 flux to the BBL presented in this study will be associated with additional OM to the BBL, and therefore lead to a temporary increased re-mineralization that offsets the increased F_θ. While the overall effect is an increase in carbon turnover, this process therefore does not result in any observable change in the decreasing O_2 trend (apparent O_2 loss rate).

4.3 Causes and controls on BBL O_2 depletion

According to Boers (2005), for BBL O_2 to decrease throughout the stratified season, there must be suitable physical conditions, biomass production, nutrient input and continued benthic O_2 uptake. SUR, and thus the sediment nutrient release and organic carbon mineralization have been shown to be strongly tidal-driven (McGinnis et al., 2014). Therefore, we briefly discuss the potential tidal impact driving the overall carbon cycling and suggest factors that may promote the development of lower BBL O_2 concentrations during the stratification period.

Tidal forcing on diapycnal constituent fluxes and primary production have been explored by e.g., Sharples et al. (2007, 2008). The authors showed that spring-neap tide drives nutrient fluxes between the BBL and the DCM at the thermocline, as well as the carbon export. Based on our velocity measurements and estimated O_2 fluxes, we can also expect similar patterns corresponding to semidiurnal tidal fluctuations. Blauw et al. (2012) investigated fluctuating phytoplankton concentrations in relation to tidal drivers and found in the southern North Sea that chlorophyll fluctuations correlated with the typical tidal current speed periods, the semidiurnal tidal cycle, in addition to

BGD
12, 9905–9934, 2015

the day-night and spring-neap periods. During most of the year, chlorophyll and suspended particulate matter fluctuated in phase with tidal current speed, and indicated alternating periods of sinking and vertical mixing of algae and suspended matter with tidal cycles. Thus, these results suggest that we can expect the semidiurnal tidal-driven export of carbon and O_2 from the DCM to the BBL, as well as entrainment of nutrients, that strongly vary based on a timescale related to the semi-diurnal tidal cycle, in addition to the spring-neap tidal cycles.

The flux of O_2 from the DCM production zone downward to the BBL should largely regulate how low the O_2 levels become during the stratification period. If there is little isolation between the zone of production and the zone of mineralization, then the net O_2 production and O_2 utilization would nearly balance. However, historically decreasing BBL O_2 concentrations within the North Sea (Queste et al., 2013) point to an increasing disconnect between the main O_2 production zone and the mineralization zones. Greenwood et al. (2010) state that stratification is an important factor which determines susceptibility to O_2 depletion, especially in their nearby study site Oyster Grounds.

Surveys on the North Sea have shown that the regions with the lowest BBL O_2 concentrations are generally characterized by the strongest stratification (see Queste et al., 2012), and the lowest reported values ($\sim 100\,\mu mol\,kg^{-1}$) were also reported to occur during particularly calm and warm weather (see Boers, 2005; Weston et al., 2008). Strong gradients in the thermocline are suggested to limit the O_2 flux to the BBL (Weston et al., 2008), and point to the potential future O_2 depletion resulting from increasing temperatures leading to both stronger stratification and a longer stratification season (Lowe et al., 2009). However, it could be expected that if O_2 fluxes between the DCM and BBL were suppressed, then the upward nutrient fluxes would be similarly suppressed, thus inhibiting primary production and therefore not resulting in observed O_2 deficits.

BGD
12, 9905–9934, 2015

4.4 Biological perspective

The occurrence of stronger stratification might have much larger implications than presently thought, since reduced turbulent mixing will alter algal populations (Hickman et al., 2009), potentially favoring migrating/swimming phytoplankton. An example of these migrating phytoplankton species, armored dinoflagellates, are extensively found in the DCM of the central and northern North Sea during the summer months; their abundance was found to be largely determined by the local hydrodynamic conditions (Reid et al., 1990). In calm conditions, which are typically associated with stronger stratification, there are often blooms of migrating dinoflagellates which have access to the large nutrient pool in the deeper water and can therefore out-compete non-migrating species for both light and nutrients. Stronger turbulent mixing, in contrast, has been suggested to interfere with their swimming abilities and thus favoring other algal species (see Jephson et al., 2012 and references therein).

Migration-driven movement of the DCM higher in the thermocline, even by a few meters, means that the O_2 production will be shifted higher in the thermocline. For example, assuming our previous values of SUR and R in Eq. (6), but reducing F_θ by half results in a nearly 3 × increase in the apparent O_2 loss rate. Therefore, the combined effects of reduced turbulent O_2 flux and a reduced O_2 gradient at the base of the thermocline, will both further isolate the BBL from this potential O_2 supply while maintaining similar rates of carbon export (settling armored dinoflagellates). We speculate that this mechanism could therefore provide a further loss of O_2 connectivity as the amount of production would remain approximately the same, but the supply of O_2 to the BBL would be substantially reduced.

The largest effect would most likely occur due to a potential isolation between the major zone of productivity and the zone of respiration. A similar effect would be expected to occur, should the North Sea become more turbid in the future. Obviously, some O_2 loss in the bottom water would occur from exported organic matter from the surface layer; however, this value is low in comparison due to overall nutrient limita-

BGD
12, 9905–9934, 2015

tions. In fact, lateral nutrient import can be neglected given the site's distance from the shoreline. Similarly, allochthonous organic carbon would not likely reach these distances, resulting in a negligible contribution to oxygen uptake.

Our findings suggest there is a complex interplay between the tidally-driven physics, water column structure, and biogeochemical cycling in the central North Sea. In this study, we proposed a mechanism that may account for the observed decreasing O_2 levels in the North Sea water column, however, further detailed studies are obviously necessary to validate and fully quantify this effect.

Acknowledgements. We are thankful to the captain and crewmembers of the R/V *Celtic Explorer* for their outstanding collaboration and support during the survey, Uwe Koy and Rudolf Link for their logistic support, and Jens Schafstall, Tim Fischer and Markus Faulhaber for their help in data collection and processing. We are grateful for the technical development and support in deployment of the benthic chamber by Ralf Schwarz, Sergiy Cherednichenko and the ROV Kiel 6000 team. Financial support was provided by the Sonderforschungsbereich (SFB) 754 "Climate–Biogeochemisty in the Tropical Ocean", SFB 574 "Volatiles and Fluids in Subduction Zones", and by the Excellence Cluster "Future Ocean" (project 2009/1 CP 0915, LR), supported by the Deutsche Forschungsgemeinschaft (DFG). Additional founding was provided by the National Environmental Research Council (NERC, project NE/J011681/1). The cruise was financed by Wintershall within the Fluid and Gas Seepage in the Southern German North Sea (SDNS) project.

The article processing charges for this open-access publication were covered by a Research Centre of the Helmholtz Association.

References

Batchelor, G. K.: The Theory of Homogeneous Turbulence, Cambridge University Press, Cambridge, 1953.

Best, M. A., Wither, A. W., and Coates, S.: Dissolved oxygen as a physico-chemical supporting element in the Water Framework Directive, Mar. Pollut. Bull., 55, 53–64, doi:10.1016/j.marpolbul.2006.08.037, 2005.

BGD
12, 9905–9934, 2015

Blauw, A. N., Beninca, E., Laane, R. W. P. M., Greenwood, N., and Huisman, J.: Dancing with the tides: fluctuations of coastal phytoplankton orchestrated by different oscillatory modes of the tidal cycle, Plos One, 7, e49319, doi:10.1371/journal.pone.0049319, 2012.
Boers, M.: Effects of a deep sand extraction pit, Final Report of the PUTMOR Measurements at the Lowered Dump Site, Rijkswaterstaat, the Netherlands, RIKZ/2005.001, 87, 2005.
Bouffard, D., Ackerman, J. D., and Boegman, L.: Factors affecting the development and dynamics of hypoxia in a large shallow stratified lake: hourly to seasonal patterns, Water Resour. Res., 49, 2380–2394, doi:10.1002/wrcr.20241, 2013.
Burchard, H. and Rippeth, T. P.: Generation of bulk shear spikes in shallow stratified tidal seas, J. Phys. Oceanogr., 39, 969–985, doi:10.1175/2008JPO4074.1, 2009.
Canfield, D. E.: Organic matter oxidation in marine sediments, in: Interactions of C, N, P and S Biogeochemical Cycles and Global Change, edited by: Wollast, R., Mackenzie, F. T., and Chou, L., Springer, Berlin, 333–363, 1993.
Chan, F., Barth, J. A., Lubchenco, J., Kirincich, A., Weeks, H., Peterson, W. T., and Menge, B. A.: Emergence of anoxia in the California current large marine ecosystem, Science, 319, 920–920, doi:10.1126/Science.1149016, 2008.
Crawford, W. R. and Pena, M. A.: Declining oxygen on the British Columbia continental shelf, Atmos. Ocean., 51, 88–103, doi:10.1080/07055900.2012.753028, 2013.
Diaz, R. J.: Overview of hypoxia around the world, J. Environ. Qual., 30, 275–281, doi:10.2134/jeq2001.302275x, 2001.
Diaz, R. J. and Rosenberg, R.: Spreading dead zones and consequences for marine ecosystems, Science, 321, 926–929, doi:10.1126/Science.1156401, 2008.
Efron, B.: 1977 Rietz lecture – bootstrap methods – another look at the jackknife, Ann. Stat., 7, 1–26, 1979.
Ferrari, R. and Polzin, K. L.: Finescale structure of the T–S relation in the eastern North Atlantic, J. Phys. Oceanogr., 35, 1437–1454, doi:10.1175/JPO2763.1, 2005.
Fischer, T., Banyte, D., Brandt, P., Dengler, M., Krahmann, G., Tanhua, T., and Visbeck, M.: Diapycnal oxygen supply to the tropical North Atlantic oxygen minimum zone, Biogeosciences, 10, 5079–5093, doi:10.5194/bg-10-5079-2013, 2013.
Fofonoff, N. P.: Physical properties of seawater: a new salinity scale and equation of state for seawater, J. Geophys. Res., 90, 3332–3342, doi:10.1029/Jc090ic02p03332, 1985.
Glud, R. N.: Oxygen dynamics of marine sediments, Mar. Biol. Res., 4, 243–289, doi:10.1080/17451000801888726, 2008.

BGD
12, 9905–9934, 2015

Grantham, B. A., Chan, F., Nielsen, K. J., Fox, D. S., Barth, J. A., Huyer, A., Lubchenco, J., and Menge, B. A.: Upwelling-driven nearshore hypoxia signals ecosystem and oceanographic changes in the northeast Pacific, Nature, 429, 749–754, doi:10.1038/Nature02605, 2004.

Greenwood, N., Parker, E. R., Fernand, L., Sivyer, D. B., Weston, K., Painting, S. J., Kröger, S., Forster, R. M., Lees, H. E., Mills, D. K., and Laane, R. W. P. M.: Detection of low bottom water oxygen concentrations in the North Sea; implications for monitoring and assessment of ecosystem health, Biogeosciences, 7, 1357–1373, doi:10.5194/bg-7-1357-2010, 2010.

Hickman, A. E., Holligan, P. M., Moore, C. M., Sharples, J., Krivtsov, V., and Palmer, M. R.: Distribution and chromatic adaptation of phytoplankton within a shelf sea thermocline, Limnol. Oceanogr., 54, 525–536, doi:10.4319/lo.2009.54.2.0525, 2009.

Hovland, M. and Judd, A.: Seabed Pockmarks and Seepage: Impact on Geology, Biology and the Marine Environment, Graham and Trotman, London, 1988.

Itsweire, E. C., Osborn, T. R., and Stanton, T. P.: Horizontal distribution and characteristics of shear layers in the seasonal thermocline, J. Phys. Oceanogr., 19, 302–320, doi:10.1175/1520-0485(1989)019<0301:HDACOS>2.0.CO;2, 1989.

Ivey, G. N. and Imberger, J.: On the nature of turbulence in a stratified fluid, Part I: The energetics of mixing, J. Phys. Oceanogr., 21, 650–658, doi:10.1175/1520-0485(1991)021<0650:OTNOTI>2.0.CO;2, 1991.

Jephson, T., Carlsson, P., and Fagerberg, T.: Dominant impact of water exchange and disruption of stratification on dinoflagellate vertical distribution, Estuar. Coas. Shelf S., 112, 198–206, doi:10.1016/j.ecss.2012.07.020, 2012.

Joos, F., Plattner, G.-K., Stocker, T. F., Körtzinger, A., and Wallace, D. W. R.: Trends in marine dissolved oxygen: implications for ocean circulation changes and the carbon budget, EOS T. Am. Geophys. Un., 84, 197–204, 2003.

Keeling, R. F., Kortzinger, A., and Gruber, N.: Ocean deoxygenation in a warming world, Annu. Rev. Mar. Sci., 2, 199–229, doi:10.1146/Annurev.Marine.010908.163855, 2010.

Kemp, W. M., Testa, J. M., Conley, D. J., Gilbert, D., and Hagy, J. D.: Temporal responses of coastal hypoxia to nutrient loading and physical controls, Biogeosciences, 6, 2985–3008, doi:10.5194/bg-6-2985-2009, 2009.

Knight, P. J., Howarth, M. J., and Rippeth, T. P.: Inertial currents in the northern North Sea, J. Sea Res., 47, 269–284, doi:10.1016/S1385-1101(02)00122-3, 2002.

BGD
12, 9905–9934, 2015

Kreling, J., Bravidor, J., McGinnis, D. F., Koschorreck, M., and Lorke, A.: Physical controls of oxygen fluxes at pelagic and benthic oxyclines in a lake, Limnol. Oceanogr., 59, 1637–1650, doi:10.4319/lo.2014.59.5.1637, 2014.

Lorke, A., Umlauf, L., and Mohrholz, V.: Stratification and mixing on sloping boundaries, Geophys. Res. Lett., 35, L14610, doi:10.1029/2008GL034607, 2008.

Lowe, J. A., Howard, T. P., Pardaens, A., Tinker, J., Holt, J., Wakelin, S., Milne, G., Leake, J., Wolf, J., Horsburgh, K., Reeder, T., Jenkins, G., Ridley, J., Dye, S., and Bradley, S.: UK Climate Projections Science Report: Marine and Coastal Projections, Met Office Hadley Centre, available at: http://ukclimateprojections.metoffice.gov.uk/22530, 2009.

MacKinnon, J. A. and Gregg, M. C.: Near-inertial waves on the New England shelf: the role of evolving stratification, turbulent dissipation, and bottom drag, J. Phys. Oceanogr., 35, 2408–2424, doi:10.1175/JPO2822.1, 2005.

McGinnis, D. F., Sommer, S., Lorke, A., Glud, R. N., and Linke, P.: Quantifying tidally driven benthic oxygen exchange across permeable sediments: an aquatic eddy correlation study, J. Geophys. Res.-Oceans, 119, 6918–6932, doi:10.1002/2014JC010303, 2014.

Meyer, E. M. I., Pohlmann, T., and Wiesse, R.: Thermodynamic variability and change in the North Sea (1948–2007) derived from a multidecadal hindcast, J. Marine Syst., 86, 35–44, doi:10.1016/j.jmarsys.2011.02.001, 2011.

North Sea Task Force: North Sea Quality Status Report 1993, Oslo and Paris Commissions, ISBN 1-872349-06-4, 1993.

Osborn, T. R.: Estimates of the local rate of vertical diffusion from dissipation measurements, J. Phys. Oceanogr., 10, 83–89, doi:10.1175/1520-0485(1980)010<0083:EOTLRO>2.0.CO;2, 1980.

OSPAR (Oslo–Paris Convention for the Protection of the Marine Environment of the North-East Atlantic): EcoQO Handbook – Handbook for the Application of Ecological Quality Objectives in the North Sea, Report No.: 978-1-905859-46-7, 2nd edn., OSPAR Biodiversity Series 2009/307, available at: http://www.ospar.org/v_publications/browse.asp, 2009.

OSPAR: Quality Status Report 2010, Report No: 978-1-906840-44-0, OSPAR Commission, London, available at: http://qsr2010.ospar.org/en/index.html, 2010.

Otto, L., Zimmerman, J. T. F., Furnes, G. K., Mork, M., Saetre, R., and Becker, G.: Review of the physical oceanography of the North Sea, Neth. J. Sea Res., 26, 161–238, doi:10.1016/0077-7579(90)90090-4, 1990.

BGD
12, 9905–9934, 2015

Palmer, M. R., Rippeth, T. P., and Simpson, J. H.: An investigation of internal mixing in a seasonally stratified shelf sea, J. Geophys. Res., 113, C12005, doi:10.1029/2007JC004531, 2008.
Pingree, R. D., Holligan, P. M., and Mardell, G. T.: The effect of vertical stability on phytoplankton distributions in the summer on the Northwest European Shelf, Deep-Sea Res., 25, 1011–1028, doi:10.1016/0146-6291(78)90584-2, 1978.
Prandke, H. and Stips, A.: Test measurements with an operational microstructure-turbulence profiler: detection limit of dissipation rates, Aquat. Sci., 60, 191–209, doi:10.1007/s000270050036, 1998.
Queste, B. Y., Fernand, L., Jickells, T. D., and Heywood, K. J.: Spatial extent and historical context of North Sea oxygen depletion in August 2010, Biogeochemistry, 113, 53–68, doi:10.1007%2Fs10533-012-9729-9, 2012.
Reid, P. C., Lancelot, C., Gieskes, W. W. C., Hagmeier, E., and Weichart, G.: Phytoplankton of the North Sea and its dynamics – a review, Neth. J. Sea Res., 26, 295–331, doi:10.1016/0077-7579(90)90094-W, 1990.
Rippeth, T. P.: Mixing in seasonally stratified shelf seas: a shifting paradigm, Philos. T. R. Soc. A, 363, 2837–2854, doi:10.1098/rsta.2005.1662, 2005.
Rippeth, T. P., Simpson, J. H., Player, R., and Garcia, M. C.: Current oscillations in the diurnal-inertial band on the Catalonian Shelf in spring, Cont. Shelf Res., 22, 247–265, doi:10.1016/S0278-4343(01)00056-5, 2002.
Rippeth, T. P., Wiles, P., Palmer, M. R., Sharples, J., and Tweddle, J.: The diapcynal nutrient flux and shear-induced diapcynal mixing in the seasonally stratified western Irish Sea, Cont. Shelf Res., 29, 1580–1587, doi:10.1016/j.csr.2009.04.009, 2009.
Schafstall, J., Dengler, M., Brandt, P., and Bange, H.: Tidal-induced mixing and diapycnal nutrient fluxes in the Mauritanian upwelling region, J. Geophys. Res.-Oceans, 115, C10014, doi:10.1029/2009jc005940, 2010.
Schneider von Deimling, J., Greinert, J., Chapman, N. R., Rabbel, W., and Linke, P.: Acoustic imaging of natural gas bubble ebullition in the North Sea: sensing the temporal, spatial and activity variability, Limnol. Oceanogr.-Meth., 8, 155–171, doi:10.4319/lom.2010.8.155, 2010.
Sharples, J.: Potential impacts of the spring-neap tidal cycle on shelf sea primary production, J. Plankton Res., 30, 183–197, doi:10.1093/plankt/fbm088, 2008.
Sharples, J., Moore, C. M., Rippeth, T. P., Holligan, P. M., Hydes, D. J., Fisher, N. R., and Simpson, J. H.: Phytoplankton distribution and survival in the thermocline, Limnol. Oceanogr., 46, 486–496, doi:10.4319/lo.2001.46.3.0486, 2001.

BGD
12, 9905–9934, 2015

Sharples, J., Tweddle, J. F., Green, J. A. M., Palmer, M. R., Kim, Y. N., Hickman, A. E. Holligan, P. M., Moore, C. M., Rippeth, T. P., Simpson, J. H., and Krivtsov, V.: Spring-neap modulation of internal tide mixing and vertical nitrate fluxes at a shelf edge in summer, Limnol. Oceanogr., 52, 1735–1747, doi:10.4319/lo.2007.52.5.1735, 2007.

Shih, L. H., Koseff, J. R., Ivey, G. N., and Ferziger, J. H.: Parameterization of turbulent fluxes and scales using homogeneous sheared stably stratified turbulence simulations, J. Fluid Mech., 525, 193–214, doi:10.1017/S0022112004002587, 2005.

Simpson, J. H. and Tinker, J. P.: A test of the influence of tidal stream polarity on the structure of turbulent dissipation, Cont. Shelf Res., 29, 320–332, doi:10.1016/j.csr.2007.05.013, 2009.

Smyth, W. D., Moum, J. N., and Caldwell, D. R.: The efficiency of mixing in turbulent patches: inferences from direct simulations and microstructure observations, J. Phys. Oceanogr., 31, 1969–1992, doi:10.1175/1520-0485(2001)031<1969:TEOMIT>2.0.CO;2, 2001.

St. Laurent, L. and Schmitt, R. W.: The contribution of salt fingers to vertical mixing in the North Atlantic Tracer Release Experiment, J. Phys. Oceanogr., 29, 1404–1424, 1999.

van Haren, H., Mass, L., Zimmerman, J. T. R., Ridderinkhof, H., and Malschaert, H.: Strong inertial currents and marginal internal wave stability in the central North Sea, Geophys. Res. Lett., 26, 2993–2996, doi:10.1029/1999GL002352, 1999.

Vaquer-Sunyer, R. and Duarte, C. M.: Thresholds of hypoxia for marine biodiversity, P. Natl. Acad. Sci. USA, 105, 15452–15457, doi:10.1073/pnas.0803833105, 2008.

Weston, K., Fernand, L., Mills, D. K., Delahunty, R., and Brown, J.: Primary production in the deep chlorophyll maximum of the central North Sea, J. Plankton Res., 27, 909–922, doi:10.1093/plankt/fbi064, 2005.

Weston, K., Greenwood, N., Fernand, L., Pearce, D. J., and Sivyer, D. B.: Environmental controls on phytoplankton community composition in the Thames Plume, U.K., J. Sea Res., 60, 246–254, doi:10.1016/j.seares.2008.09.003, 2008.

BGD
12, 9905–9934, 2015

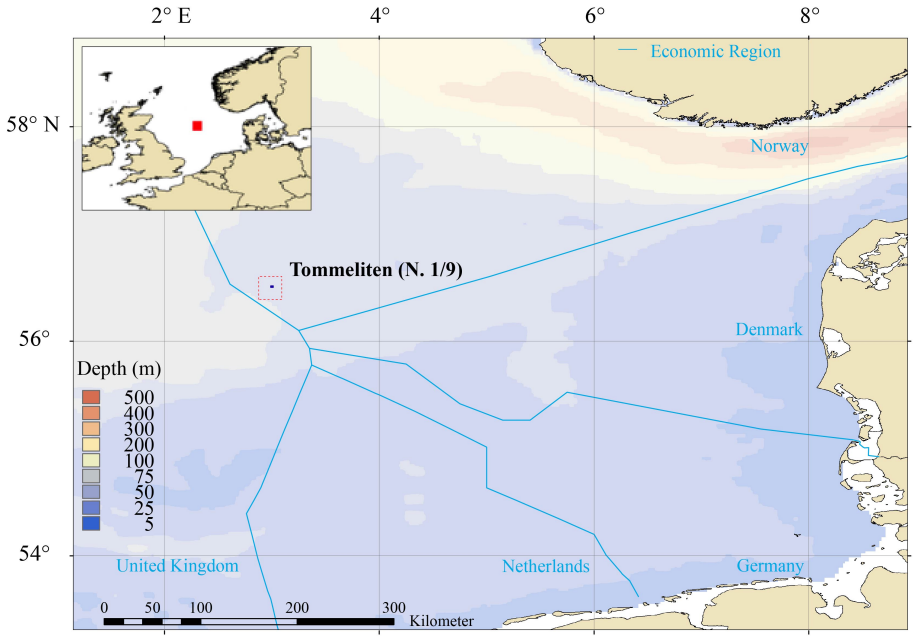

Figure 1. Map of the North Sea indicating the water depths and location of the Tommeliten site as well as the borders of the economical regions of the surrounding European countries.

BGD
12, 9905–9934, 2015

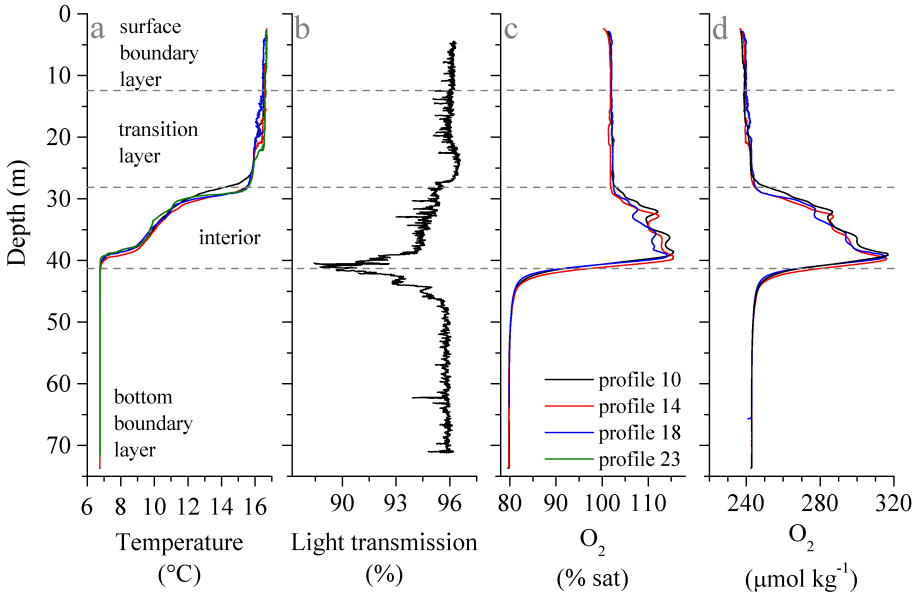

Figure 2. Selected water column profiles based on based on high-resolution MSS profiles **(a, c, d)** and ship CTD profile **(b)**. **(a)** Potential temperature profiles with inferred temperature layers. **(b)** Light transmission profile. **(c, d)** O_2 saturation profiles and associated absolute concentrations.

BGD
12, 9905–9934, 2015

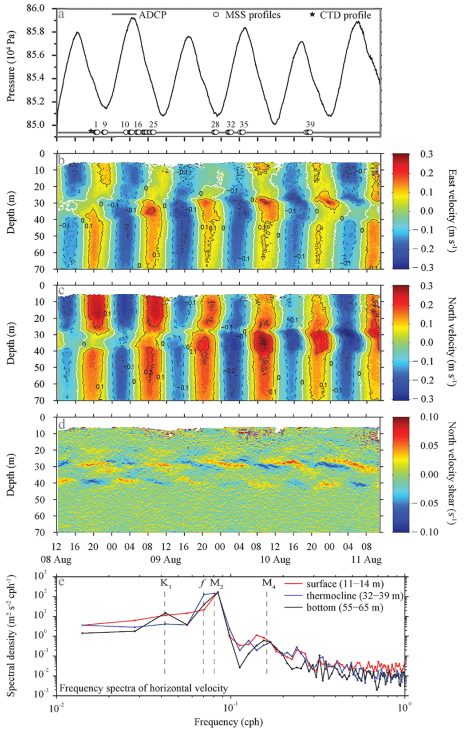

Figure 3. Current regime at the Tommeliten site from ADCP measurements **(a–d)** and spectral analysis **(e)**. **(a)** Sea surface elevation relative to average level during the observational period (elevation = 0 m) and schedule of different instrument deployments. Numbers on the MSS markers indicate the profile number. **(b, c)** Horizontal velocities, showing 20 min averaged east **(b)** and north **(c)** velocities. **(d)** Vertical shear of North velocity, dv/dz, calculated from the ADCP velocity data (see panels **b**, **c**). Note that panels **(a–d)** have the same time axis. **(e)** Frequency spectra of horizontal velocity calculated from the ADCP data for selected depth ranges for the SBL (surface; red line), thermocline (blue line), and BBL (bottom; black line). The inertial f as well as the K_1, M_2 and M_4 frequencies are marked.

BGD
12, 9905–9934, 2015

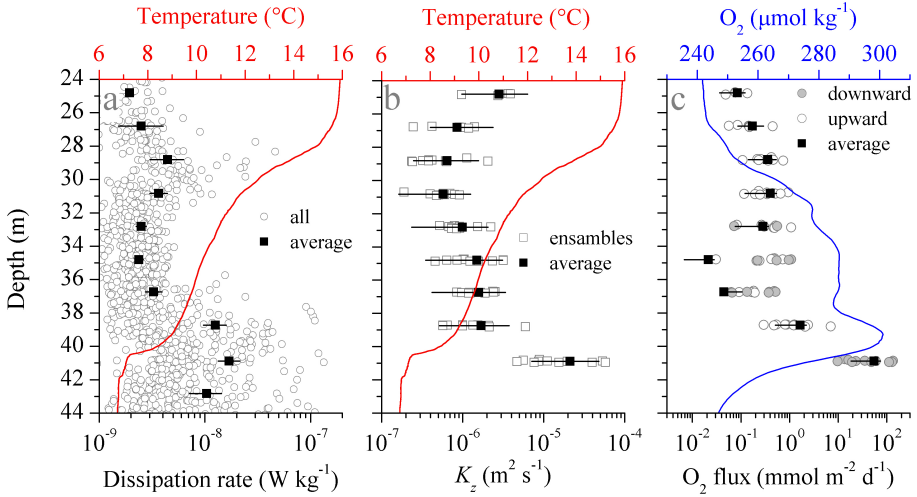

Figure 4. Overview of turbulent transport and O_2 fluxes within the interior (defined in Fig. 2). Each panel is overlaid with temperature **(a, b)** and O_2 concentration **(c)** profiles. **(a)** Dissipation from all profiles (open dots) together with the arithmetic mean (solid squares). **(b)** Average vertical eddy diffusion coefficient K_z with uncertainties bars as well as the K_z values for every ensemble (open squares), which represent the average over 3 to 4 consecutive profiles. **(c)** Calculated average O_2 flux over 2 m bins with the respective uncertainties intervals (solid square and black line). The values for each profile cluster are shown both downward and upward fluxes (grey solid and open dots, respectively).

BGD
12, 9905–9934, 2015

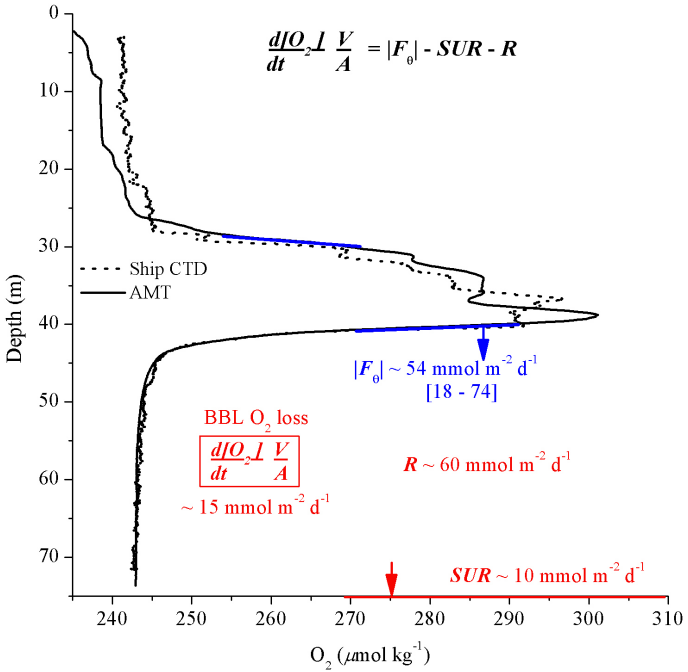

Figure 5. Main O_2 fluxes in this study. The ranges shown for the interior O_2 fluxes refer to the associated uncertainty and intermittency levels. The sediment O_2 uptake rates (SUR) are based on eddy correlation (EC) measurements (McGinnis et al., 2014), while central North Sea apparent BBL O_2 loss is based on Greenwood et al. (2010) and this study. Representative O_2 profiles are based on the AMT sensor on the MSS profiler (solid line) and ship CTD (dotted line). Note that while the O_2 profiles showed differences in absolute concentration within the thermocline, the actual O_2 gradients within the thermocline-BBL oxycline are comparable.

BGD
12, 9905–9934, 2015